Journal of ELECTRICAL ENGINEERING, VOL. 54, NO. 1-2, 2003, 3–12

A PERFORMANCE EVALUATION METHOD FOR GEOMETRY–DRIVEN DIFFUSION FILTERS

Ivan Bajla [*] — **Igor Holländer** [*] — **Viktor Witkovský** [**]

A novel quantitative method is proposed for the algorithm performance evaluation for geometry-driven diffusion (GDD) filtering methods. It is based on a probabilistic model of stepwise constant image corrupted by uncorrelated Gaussian noise. The maximum likelihood estimates of the distribution parameters of the random variable derived from intensity gradient are used for characterization of staircase image artifacts in diffused images. The proposed evaluation technique incorporates a "gold standard" of the GDD algorithms, defined as a diffusion process governed by ideal values of conductance. A phantom mimicing an MR brain scan is used as a sample data set.

K e y w o r d s: Geometry-driven diffusion, Image filtering, Empirical evaluation of computer vision algorithms, Stochastic modeling

1 INTRODUCTION

Geometry-driven diffusion (GDD) (or anisotropic diffusion) algorithms have justified themselves within the class of image filtering methods ([1], [2], [3]). Theoretical exploration of the mathematical problems related to these nonlinear filters advanced considerably in the recent decade (*eg* [4], [5], [6]). Particular aspects of their discrete implementation and quantitative methods for performance evaluation have been addressed in several papers [7], [8], [9], [10] and the importance of such techniques for computer vision community have already been established in various works [11], [12], [13]. In applications, a number of authors stick to the original Perona and Malik's anisotropic diffusion scheme [14], but numerous derived, similar and/or improved algorithmic approaches have appeared in the meantime in [15], [16], [17], [18], [19], [20], [21], [22]. Novel application areas for GDD have emerged which prove the power of these filters for both 2D and 3D data filtering (*eg* 3D surface smoothing in [23] and vector field visualization in [24]). This makes the need of a systematic evaluation and mutual comparison of the GDD filters even more relevant.

The performance of the filtering algorithms (other than computational complexity) is usually measured in terms of improvement of the signal-to-noise ratio. Nevertheless, the major beneficial effect of the GDD methods, which is in nearly all cases motivating their application, is the edge-preserving image smoothing. A general GDD evaluation approach should therefore measure this effect.

Since the GDD methods in computer vision are based on the analogy to the physical process of diffusion, it is possible to define their performance limit. In physical terms, the diffusion process converges to the state where a quantity (such as concentration, temperature etc.) is totally homogenized within the given spatial boundaries (such as the volume of the container). Different regularization schemes for the partial differential equation of the diffusion, as well as various parametrizations introduce different approximations of the continuous model, which may prevent the numerical solution to reach the theoretical limit of total homogenization of image regions (although it can be tuned to get very close to this limit so that it is acceptable in practical applications). In this paper we propose a scheme for evaluation of edge-preserving smoothing effects and accompanying artifacts produced by GDD filters. The evaluation is restricted to images which can be modelled by a piecewise constant artificial phantom corrupted by uncorrelated Gaussian noise which, however, constitute a wide class of images occurring in practice, especially in medical imaging. Since region boundaries and interiors are known *a priori* in this phantom, limit diffusion process (with maximum conductance within the interiors and minimum conductance across boundaries) can be applied and the result of this filtering can be taken for the performance standard. We introduce a statistical parameter, which is an objective quantification of the visually perceived smoothing effect and, at the same time, it is sensitive to typical adverse effects of the GDD filters like staircase artifacts.

To illustrate the evaluation method, we chose a magnetic resonance (MR) scan for which the piecewise constant model is natural because it is implied by the visualized object — in a tomographic scan, the different image regions represent different tissues. What is more, a plausible noise model is available for MR scans ([25], [26], [27]). The choice of the brain MR scan has also been partially motivated by the application background of the authors ([10], [22], [28]), but it is not limiting the applicability of the presented method in any way.

[*] ARC Seibersdorf research, Department of High Performance Image Processing, A-2444 Seibersdorf, Austria, ivan.bajla@arcs.ac.at

[**] Institute of Measurement Science, Slovak Academy of Sciences (IMS SAS), 841 04 Bratislava, Slovakia

ISSN 1335-3632

2 NONLINEAR GEOMETRY–DRIVEN DIFFUSION METHODS OF IMAGE FILTERING

The basic mathematical model of the GDD filtering proposed by Perona and Malik [14] is described by the partial differential equation (PDE)

$$\partial I/\partial t = \operatorname{div}\left[c\left(|\nabla I(x,y,t)|\right)\nabla I(x,y,t)\right], \qquad (1)$$

where $|\nabla I(x,y,t)|$ is the gradient magnitude of an image intensity function $I(x,y,t)$, the conductance $c()$ is a spatial function of the gradient magnitude that may vary in time t. The rapidly decreasing conductivities in the model of Perona and Malik, as well as in other image diffusion models create ill-posed processes, as pointed out in [4]. To avoid this, a regularization of the diffusion proposed by Catté is used. Different numerical schemes of PDE discretization have different impact on the accuracy of computations which have been studied in several papers, *eg* [9], [29], [3]. Since in computer vision application GDD is used for digital image filtering, the final smoothing effect in an image is exactly what we intend to measure in the evaluation scheme.

Nonlinear geometry-driven diffusion methods derived from this parabolic partial differential equation with the scalar-valued diffusivity (conductance), that is given as a function of the differential structure of the evolving image itself, constitute a wide class of diffusion image filtering methods which are used in various applications, including those of medical imaging. The essential goal of these methods is edge-preserving noise suppression. The application of these methods to a phantom image, comprising piecewise constant intensity regions corrupted by noise, would allow to evaluate the achieved results in terms of the independent homogenization of the individual region interiors and preservation of intensities on given boundaries.

3 STOCHASTIC MODEL OF THE PIECEWISE CONSTANT IMAGE PHANTOM CORRUPTED BY GAUSSIAN NOISE

We are interested in developing an evaluation technique for individual GDD filters that would quantify the visual appearance of the resulting phantom images. We base it on the stochastic model of an appropriate quantity derived from image intensities. Considering an image phantom with *a priori* known boundaries enables us to build a reasonably simplified stochastic model that features two important aspects: (i) the formula of the random variable and (ii) the choice of the specific pixel subsets as random variable samples. For any two adjacent regions in the piecewise constant image phantom an image model consisting of two homogeneous regions, Ω_1 and Ω_2, having different constant pixel intensities can be considered. Let this image be corrupted by uncorrelated Gaussian noise so that the pixel intensities in Ω_1 region have the probability distribution $X_1 \sim N(\mu_1, \sigma_1^2)$. Similarly, the pixel intensities in Ω_2 region have the probability distribution $X_2 \sim N(\mu_2, \sigma_2^2)$. For simplicity, in the following we will assume that $\sigma_1^2 = \sigma_2^2 = \sigma^2$. So, the intensity value in a given pixel can be thought of as a realization of a random variable X_1 in Ω_1 and X_2 in Ω_2.

Let us take two arbitrary pixels within Ω_1. The intensity values in these pixels are realizations of two independent and identically distributed random variables, say $X_1' \sim N(\mu_1, \sigma^2)$ and $X_1'' \sim N(\mu_1, \sigma^2)$. The difference between intensity values is defined by $\Delta_1 = X_1' - X_1''$. Under given assumptions $\Delta_1 \sim N(0, 2\sigma^2)$. Similarly we can define $\Delta_2 = X_2' - X_2''$, the difference of intensity values of two pixels from Ω_2. Under the assumption that $X_2' \sim N(\mu_2, \sigma^2)$ and $X_2'' \sim N(\mu_2, \sigma^2)$ we get $\Delta_2 \sim N(0, 2\sigma^2)$.

Now, we will consider the 4-neighborhood of the pixel with indices (i,j). We define the differences of intensity values

$$\begin{aligned} \Delta_i(i,j) &= X(i+1,j) - X(i-1,j), \\ \Delta_j(i,j) &= X(i,j+1) - X(i,j-1), \end{aligned} \qquad (2)$$

where the independent random variables $X(i-1,j)$, $X(i+1,j)$, $X(i,j-1)$, and $X(i,j+1)$ represent intensity values in pixels belonging to the 4-neighborhood of the pixel with indices (i,j). The distributions of $\Delta_i(i,j)$ and $\Delta_j(i,j)$ depend on the distributions of X's. There are just two possibilities for the distribution of the particular X. If X is from Ω_1 then $X \sim N(\mu_1, \sigma^2)$, if X is from Ω_2 then $X \sim N(\mu_2, \sigma^2)$. The distribution of the central digital gradient magnitude (simply gradient) is of interest:

$$G' = G'(i,j) = \frac{1}{2}\sqrt{\Delta_i^2(i,j) + \Delta_j^2(i,j)}\,. \qquad (3)$$

4 ESTIMATES OF PROBABILITY DISTRIBUTION PARAMETERS FOR FILTERING RESULTS CHARACTERIZATION

The squared gradient is the argument of the conductance function and, moreover, it is suitable for stochastic treatment. Therefore, we will consider the random variable $(G')^2 = \frac{1}{4}\big(\Delta_i^2(i,j) + \Delta_j^2(i,j)\big)$ instead of the variable G'. Herefrom we denote $(G')^2 = G$. The following stochastic model is strictly valid only for the initial image. Yet, in our experiments described below, this model (using maximum likelihood estimation) proved to be reasonably robust even after iterations which violate the assumption on neighbor pixel independence as well as on the normal distribution. More importantly, it proved to perform well as a vehicle to the quantification of the filtering process.

In our image model we admit only four different cases of the relation between the pixels in the 4-neighborhood

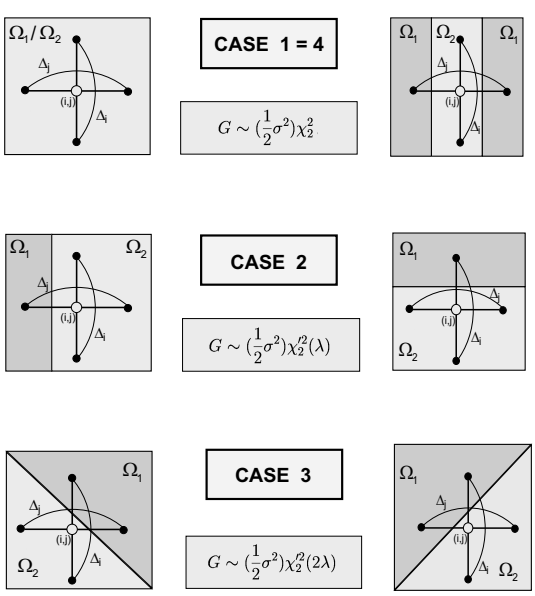

Fig. 1. The scheme of three possible types of neighboring regions for the 4-pixel neighborhood and the corresponding distributions of the quantity G.

and the neighboring regions Ω_1, Ω_2. Therefore, the individual probability distribution should be derived for each such case.

Case 1: All pixels in the 4-neighborhood come from the same region Ω_1 or Ω_2. Then $\Delta_i \sim N(0, 2\sigma^2)$ and $\Delta_j \sim N(0, 2\sigma^2)$ are independent random variables, as are the squares $\Delta_i^2 \sim (2\sigma^2)\chi_1^2(\lambda)$ and $\Delta_j^2 \sim (2\sigma^2)\chi_1^2(\lambda)$. Consequently, $G \sim \frac{1}{4}(2\sigma^2)\chi_2^2 = (\frac{1}{2}\sigma^2)\chi_2^2$, where χ_2^2 denotes a random variable with central chi-square distribution and two degrees of freedom. Notice that the theoretical expectation of G in this case is $E(G) = \sigma^2$ and variance $\mathrm{Var}(G) = \sigma^4$.

Case 2: If $X(i+1, j)$ and $X(i-1, j)$ come from the same region, say Ω_1, but $X(i, j+1)$ and $X(i, j-1)$ come from different regions, say Ω_1 and Ω_2, then $\Delta_i \sim N(0, 2\sigma^2)$ and $\Delta_j \sim N(\mu_1 - \mu_2, 2\sigma^2)$, and $\Delta_i^2 \sim (2\sigma^2)\chi_1^2$ and $\Delta_j^2 \sim (2\sigma^2)\chi_1'^2(\lambda)$ are independent random variables. The first one has a distribution proportional to the central chi-square distribution with one degree of freedom, the second one has a distribution proportional to the noncentral chi-square distribution with one degree of freedom and with the noncentrality parameter $\lambda = (\mu_1 - \mu_2)^2/(2\sigma^2)$. Finally, we get that $G \sim (\frac{1}{2}\sigma^2)\chi_2'^2(\lambda)$ is a random variable with distribution proportional to the noncentral chi-square distribution with two degrees of freedom and the noncentrality parameter $\lambda = (\mu_1 - \mu_2)^2/(2\sigma^2)$. Notice that the distribution of G does not depend on particular ordering of regions Ω_1 and Ω_2 in the possible directions. Here, the expectation of G is $E(G) = \frac{1}{2}\sigma^2(2+\lambda)$, and variance $\mathrm{Var}(G) = \sigma^4(1+\lambda)$.

Case 3: If $X(i+1, j)$ and $X(i-1, j)$, and also $X(i, j+1)$ and $X(i, j-1)$, come from different regions, say Ω_1 and Ω_2, then $\Delta_i \sim N(\mu_1 - \mu_2, 2\sigma^2)$ and $\Delta_j \sim N(\mu_1 - \mu_2, 2\sigma^2)$. Consequently, $\Delta_i^2 \sim (2\sigma^2)\chi_1'^2(\lambda)$ and $\Delta_j^2 \sim (2\sigma^2)\chi_1'^2(\lambda)$ are independent random variables with distributions proportional to the noncentral chi-square distribution with one degree of freedom and with the noncentrality parameter $\lambda = (\mu_1 - \mu_2)^2/(2\sigma^2)$. Then, $G \sim (\frac{1}{2}\sigma^2)\chi_2'^2(2\lambda)$ is a random variable with distribution proportional to the noncentral chi-square distribution with two degrees of freedom and the noncentrality parameter $(\mu_1 - \mu_2)^2/\sigma^2$. The expectation of G is $E(G) = \sigma^2(1+\lambda)$, and variance $\mathrm{Var}(G) = \sigma^4(1+2\lambda)$.

Case 4: If $X(i+1, j)$ and $X(i-1, j)$ come from the same region, say Ω_1, and $X(i, j+1)$ and $X(i, j-1)$ come also from the same region, however different from Ω_1, say Ω_2, then $\Delta_i \sim N(0, 2\sigma^2)$ and $\Delta_j \sim N(0, 2\sigma^2)$. Consequently, the **Case 4** reduces just to the **Case 1**.

In Fig. 1 all three discussed cases are illustrated. In all cases, λ and σ^2 remain unknown parameters. If we assume that we have a random sample of squared gradients from one of the three particular cases, then the maximum likelihood (ML) estimation of the parameters is of interest. The derivation of these estimates can be found in Appendix.

5 DIFFUSION–LIKE IDEAL FILTERING OF A NOISE CORRUPTED PIECEWISE CONSTANT IMAGE PHANTOM

The conductance is a specific function with extreme values 0, 1 which represent the membership of the raster point to a region interior or region boundary, given by the *a priori* partitioned phantom image. Therefore, considering the discrete diffusion formula with the extremal values of the conductance in each diffusion iteration may provide us with additional information on filtering limits of the discrete diffusion process in the given image. The filtering effects in output images depend more on the discrete conductance implementation than on the type and/or numerical accuracy of the spatial discretization. Thus, using the explicit first-order scheme for derivation of the filtering limits is in no way inferior to implicit, semi-implicit, or additive operator splitting schemes (AOS), *eg* [3].

Let us consider the expression (see *eg* [7] or [14]) of the scheme, which is given for an arbitrary pixel $I(i, j)$:

$$I_{ij}^{t+1} = I_{ij}^t + \tau[c_N \cdot D_N I^t + c_S \cdot D_S I^t + c_W \cdot D_W I^t + c_E \cdot D_E I^t], \tag{4}$$

where I_{ij}^{t+1} is the transformed intensity in the $t+1$-th iteration and I_{ij}^t is a result of the previous iteration t, τ is the time step. The terms $D_X I^t$, denote the intensity differences for four neighbors in the 4-neighborhood of the central pixel $I(i, j)$, *ie*, $D_N I^t = I(i-1, j) - I(i, j)$; $D_S I^t = I(i+1, j) - I(i, j)$; *etc.* In the evaluation studies the formula is to be applied to the noisy image phantom with *a priori* known region interiors and boundaries. For the diffusion method being evaluated first the conductances in the pixels are calculated which take real values

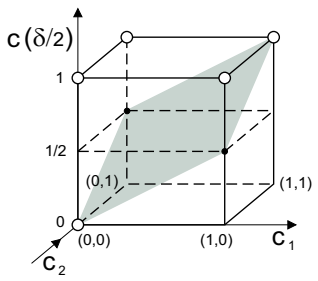

Fig. 2. Linear interpolation of the conductance values $c(\delta/2)$ from c_1, c_2 of the adjacent pixels.

from the interval $(0, 1)$. Here, the conductance function can be interpreted as an inverse-valued edge indicator (*ie*, an edge is indicated by a number approaching 0, ideally equal to 0). If we treat the formula as a local operator, the quantities c_X can be interpreted as weighting coefficients of the corresponding differences $D_X I$.

In an ideal case, for which the values of the conductances are calculated as binary attributes of pixel membership to region interior or boundary, we would expect extreme contributions from the neighboring pixels. Obviously, this is unreachable in the explicit diffusion scheme, since even in the case of extremal values of conductances the values c_X always represent the interpolated (arithmetic mean is usually used) conductance values in the $\delta/2$-subraster of the δ-raster (δ denotes the size of the conventional squared raster, see Fig. 2). An analogous characterization applies to implicit diffusion formulae, since all of them comprise interpolated values of the corresponding conductances (see *eg* [20]). For a piecewise constant image phantom an *internal* pixel $v_m \in \Omega_m$ is defined as the pixel for which all pixels from its 4-neighborhood belong to the same region Ω_m. The pixel $h_m \in \Omega_m$ is called *boundary* pixel of the region Ω_m, if at least one of its four neighbors belongs to a different region Ω_n. For any two neighboring regions Ω_m, Ω_n of the phantom the following adjacency pairs are possible: $(v_m, v_m), (v_m, h_m), (h_m, h_m), (h_m, h_n)$. Two reflective relations $(h_m, v_m), (h_n, h_m)$ do not constitute extra cases and therefore we will exclude them from our consideration. On the other side it is obvious that the couples (v_m, v_n) and (v_m, h_n) do not exist in our model.

Table 1. The values of the weights w_X in FILTIDEAL filtering and conductances $c(\,)$ in DIFIDEAL diffusion.

adjacency pixel pairs	weights w_X	$c_1(\delta)$, $c_2(\delta)$	$c(\delta/2)$
(v_m, v_m)	1	$c_1 = 1$, $c_2 = 1$	1
(v_m, h_m)	1	$c_1 = 1$, $c_2 = 0$	1/2
(h_m, h_m)	1	$c_1 = 0$, $c_2 = 0$	0
(h_m, h_n)	0	$c_1 = 0$, $c_2 = 0$	0

As a model of limits of the diffusion filtering applied to a piecewise constant noise-corrupted image phantom we suggest an iterative diffusion-like operator. The operator itself uses an explicit diffusion formula, but a similar approach can be used for implicit schemes. Formally, the operator is identical to the diffusion formula (4):

$$I_{ij}^{t+1} = I_{ij}^{t} + \tau[w_N \cdot D_N I^t + w_S \cdot D_S I^t + w_W \cdot D_W I^t + w_E \cdot D_E I^t]\,. \quad (5)$$

Here, however, the coefficients w_N, w_S, w_W, w_E denote the weights of intensity increments from adjacent pixels which are given in Table 1. In the Table we also summarize the possible values of the interpolated conductances (in $\delta/2$-raster) for ideal conductances $c_1(\delta), c_2(\delta)$ in any adjacent pixels in the neighborhood.

We introduce the following two concepts:

- *Ideal diffusion* (DIFIDEAL) is an iterative GDD process over the input image with known region boundaries that is governed by (4) with the conductances $c_X(\delta/2)$, dependent on the pixel adjacency type given in Table 1.
- *Diffusion-like ideal filtering* (FILTIDEAL) is an iterative filtering of the input image with known region boundaries that is governed by (5) with weights w_X given in Table 1.

The difference between the ideal diffusion DIFIDEAL and the diffusion-like ideal filtering FILTIDEAL is straightforward. Namely, in the case of (v_m, h_m) the best value of conductance approximation reachable in cases $(c_1, c_2) = (1, 0)$ or $(0, 1)$ is $c(\delta/2) = 1/2$. In the case of (h_m, h_m) we get zero increment in the diffusion scheme (4), *ie* no smoothing is possible within the boundary pixels of one region. Here $c(\delta/2)$ corresponds to conductance values c_X for $X = N,\ S,\ W,\ E$. It can also be noted from Table 1 that smoothing in the FILTIDEAL case is allowed for all kinds of adjacent pixels within the given phantom region Ω_m. It is stopped only in the case of two adjacent boundary pixels from distinct regions Ω_m, Ω_n. For each iteration of any of these iterative procedures of phantom filtering the output image represents an extremal case that cannot be achieved by any diffusion method. Therefore, the DIFIDEAL and FILTIDEAL filtering can be considered as *gold standards* for the GDD image filtering based on explicit discrete formulae. Note that the gold standards DIFIDEAL and FILTIDEAL are closely related to the isotropy of the diffusion model. Since DIFIDEAL stops diffusion along and across edges, it is a discretization of an isotropic diffusion process with a scalar-valued conductance. FILTIDEAL, on the other hand, stops diffusion across edges, but permits diffusion along edges. It can be regarded as a discrete formulation of an anisotropic diffusion process with a matrix-valued conductance.

6 IMPLEMENTATION RESULTS

Goals

In this Section we summarize the results of the implementation of the technique we have proposed for quan-

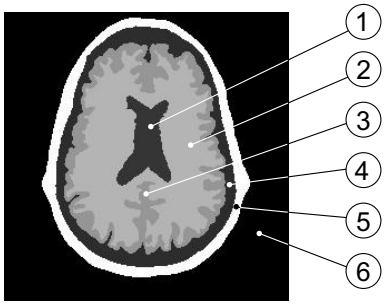

Fig. 3. The artificial phantom of the MR-head tomogram as an ideally segmented model and reference image for evaluation of the GDD filtering performance. The intensity values in individual regions are as follows: 1–ventricles(35), 2–white matter(130), 3–grey matter(80), 4–CSF(30), 5–subcutaneous fat(240), 6–image background(0).

titative evaluation of the GDD filter performance. The implementation was aimed at the following goals:

- to document the efficiency of measuring the level of region interior homogenization, being reached in the process of diffusion, by the quantity $\mathrm{Var}(G)$,
- to confirm that the application of this measure to subsets of region boundaries (of case 2 and 3, see the previous Section) provides an adequate and sensitive characterization of staircase image artifacts from which the diffused images usually suffer,
- to demonstrate that ideal diffusion processes (DIFIDEAL, FILTIDEAL) designed especially for GDD filtering of the known phantom can actually serve as *gold standards* (constituted by reference images, as well as by their numerical characteristics) for comparison of the GDD filters,
- to illustrate that the quantitative characteristic $\mathrm{Var}(G)$ applied selectively to region interiors and region boundaries are in a good accordance to visual appearance of the processed images.

Conditions

To illustrate the evaluation method, we need a piecewise constant image phantom corrupted by noise. Since the levels of detail, typical geometrical patterns as well as noise characteristics of the image may play a certain role in the evaluation, it is advisable to use a phantom mimicing the class of images from the application which the filtering methods in test should be used in. For this reason, as well as due to the background and previous work of the authors, we decided to choose a phantom image simulating a magnetic resonance (MR) scan of the human head.

The MR-head phantom is a stepwise constant image with 5 regions and 5 boundaries (Fig. 3). The phantom is corrupted by uncorrelated Gaussian noise with the parameter $\sigma = 9$. This value is chosen to reflect usual conditions of fast MR image acquisition (*eg*, via 3D FLASH method). Furthermore, using this value is in accordance with the requirement on Rician distribution of MR noisy data to become Gaussian that is given by the condition: $SNR \geq 10$ dB in a pixel Nowak(1999). Specifically, for our case with the minimum intensity 30 (region 4) we obtain $SNR = 10\log(s^2/\sigma^2) = 10\log(30^2/9^2) = 10.5$ dB that satisfies the condition for signal noise normality.

The optimum numbers of iterations in the individual methods compared had been calculated using the iteration stopping criterion proposed by us in [10], where we introduced the so-called *relative SNR* (*RSNR*) for characterization of the results of the GDD-filtering of the actual images after the $(p+1)$-th iteration $(p \geq 0)$ by the following formula:

$$ {}^{p+1}RSNR(dB) = 10 \cdot \log \frac{\sum_{i=1}^{N}\sum_{j=1}^{N}\left({}^{p+1}f_{ij}\right)^2}{\sum_{i=1}^{N}\sum_{j=1}^{N}\left({}^{p}f_{ij} - {}^{p+1}f_{ij}\right)^2}\,, \quad (6) $$

in which ${}^{p}f_{ij}$, ${}^{p+1}f_{ij}$ are the grey levels of the images resulting from the p-th and $(p+1)$-th iteration, respectively. The stopping criterion (SC) itself was defined for $p \geq 1$ as the relation

$$ {}^{p+1}SC = \frac{\left|{}^{p}RSNR - {}^{p+1}RSNR\right|}{{}^{p}RSNR} \leq thr. \quad (7) $$

The results obtained after the optimum number of diffusion iterations ensure the uniform basis of method comparison in our evaluation experiments.

Choice of the GDD filters to be compared

To demonstrate the potential of the quantity $\mathrm{Var}(G)$ to characterize the GDD filtering effects, we chose four GDD filters. The Perona and Malik's algorithm [14] (denoted in the Tables as FIXK) with the conventional exponential conductance given as follows:

$$ cond\left(|\nabla I(x,y,t)|\right) = \exp\Big\{-\Big[\frac{|\nabla I(x,y,t)|}{K}\Big]^2\Big\}, \quad (8) $$

where K denotes the relaxation parameter. In practical applications ([7], [10]) this parameter is chosen as the quantile q of the histogram of intensity gradient magnitudes. Next, in our previous paper [22] on a locally adaptive conductance (here the algorithm will be referred to as ADAPTKLKR) we compared the proposed algorithm to two different GDD algorithms, namely to Black's [19] (referred to as *Black*) and Weickert's [20] (referred to as *Weickert*) algorithms. Therefore, we involved these algorithms into our evaluation experiment. We will describe the core of these algorithms, for details see the cited papers.

Black [19] developed an approach in which the boundaries between the piecewise constant regions are considered to be "outliers" in the robust statistics interpretation. For the robust estimation procedure that estimates

a piecewise smooth image from a noisy input they proposed to use a conductance based on Tukey's biweight robust estimator:

$$g(x,\sigma) = \begin{cases} 1/2[1-(x/\sigma)^2]^2 & x \le \sigma \\ 0 & \text{otherwise,} \end{cases} \quad (9)$$

where $x = |\nabla I|$. The global parameter σ is calculated as a function of the "robust scale" σ_e: $\sigma = \sqrt{5}\,\sigma_e$. For a digital image it is computed using the gradient approximation over the entire image.

Weickert [20] proposed a rapidly decreasing conductance for GDD filters. Based on our computer experiments and personal communication with the author we proposed a modified formula for the conductance function for which good visual results are achieved for the parameter value $m = 2$:

$$g(|\nabla I_\sigma|^2) = \begin{cases} 1 & |\nabla I_\sigma| = 0 \\ 1 - \exp\left\{\frac{-C_m}{(|\nabla I_\sigma|^2/\gamma^2)^m}\right\} & |\nabla I_\sigma| > 0\,. \end{cases} \quad (10)$$

Here, by $|\nabla I_\sigma|$ the gradient magnitude of a smoothed version of the image I, obtained by convolving I with a Gaussian of standard deviation σ, is denoted. The constant C_2 is calculated in such a way that the flux $\Psi(s) = s \cdot g(s)$ is increasing for $s \in [0,\gamma]$ and decreasing for $s \in (\gamma,\infty)$, where $s = |\nabla I_\sigma|^2$. This gives $C_2 = 2.3367$. The parameter γ plays the role of a contrast adjustment: structures with $|\nabla I_\sigma| > \gamma$ are regarded as edges, while structures with $|\nabla I_\sigma| < \gamma$ are considered to belong to region interiors.

Besides the basic mode (7 diffusion iterations) the Black and Weickert algorithms have also been tested for 50 iterations and for optimum number n_{opt} of iterations given by the application of the stopping criterion (SC). For the phantom in the case of the Black algorithm $n^B_{opt} = 24$, whereas in the Weickert algorithm $n^W_{opt} = 18$.

Finally, the ADAPTKLKR algorithm (with the explicit scheme) is based on making the conductance locally adaptive. It is accomplished by (i) using a pixel dissimilarity measure $diss[i,j,t]$, defined for the pixel neighborhood, and (ii) by incorporating this local measure into the calculation of the variable relaxation parameter $K_{loc}[i,j,t]$ of the conductance $cond(G[i,j,t], K_{loc}[i,j,t])$, defined by the formula:

$$cond(G[i,j,t]) = \exp\Big\{-\frac{G[i,j,t]^2}{K_{loc}(G[i,j,t],i,j,t)^2}\Big\}, \quad (11)$$

where t denotes the t-th diffusion iteration. The variable relaxation parameter is given by the formula:

$$K_{loc}[i,j,t] = K_r - \Big(\frac{diss[i,j,t] - diss_{\min}}{diss_{\max} - diss_{\min}}\Big)^{1/p}(K_r - K_l)\,, \quad (12)$$

where the symbols K_l, K_r denote the extremum values of the relaxation parameter and the exponent $1/p$ is responsible for the rate of the transition from K_r to K_l.

Results and discussion

In Table 2 the values of $\mathrm{Var}(G)$ for the individual region interiors Ω_i are listed which have been obtained after filtering the MR-head phantom by the selected GDD filters. The results are in descending order of $\mathrm{Var}(G)$, starting with those for the noisy input phantom regions and ending with the values corresponding to two gold standard algorithms. The method B comes after the method A, if at least three region boundaries (interiors) of B exhibited lower values of $\mathrm{Var}(G)$ than those for A. Based on the values listed in these tables the following findings have been established. The quantity $\mathrm{Var}(G)$ can serve as a very sensitive measure of region interior homogenization achieved by the GDD filtering. The quantitative characterization of this effect is in a very good accordance with the visual perception of differences in region interior smoothing of the phantom obtained by different GDD filtering algorithms. Similar conclusions can be drawn for the characterization of the level of the region boundary preservation in the process of GDD filtering.

In Tables 3, 4 the values of $\mathrm{Var}(G)$ for individual region boundaries B_i (cases 2 and 3 of the distribution of $\mathrm{Var}(G)$) are listed which have been obtained in final output phantom images after GDD filtering by the algorithms compared. Minor differences in the order of $\mathrm{Var}(G)$ values for different iteration numbers of the Weickert algorithm can be explained by the fact that 50 iterations represent an extreme case. It is not reasonable to include such a quantitative characterization into the overall comparison. It can only serve here for illustration. On the other hand the slightly better result of the ADAPTKLKR, achieved for the boundary B_4, than the result of the gold standards, has been caused by numerical instability of the solution of the system of nonlinear equations (23,24).

In Fig. 4, 5 the output phantom images obtained by the application of GDD-filtering algorithms referred to in Tables 2, 3, 4 are displayed together with their fragments. The images are arranged exactly in the same order as the characteristics $\mathrm{Var}(G)$ in Tables 2, 3, 4. Based on the detailed visual analysis (the fragments displayed represent only a part of it) we can conclude that $\mathrm{Var}(G)$ properly reflects the degree of homogenization within region interiors as well as the staircase artifacts. The particular numerical values of $\mathrm{Var}(G)$ describe the differences between the distinct resulting images in a good correlation with their visual appearance.

7 CONCLUSIONS

We have presented in this paper a novel task-based algorithm performance evaluation technique related but not restricted to the geometry-driven diffusion filters. The main contribution of the paper is in the development of a probabilistic framework which is suitable for quantitative characterization of the smoothing effect in diffused

Table 2. The values of the characteristic $\mathrm{Var}(G)$ in five region interiors of the MR-head phantom calculated for the output images of individual GDD filtering methods.

GDD-f method	**Region interior (case 1)**				
	Ω_1 ventricles	Ω_2 white matter	Ω_3 grey matter	Ω_4 CSF	Ω_5 fat
number of pixels	1804	11807	4047	4551	4120
original	6 773.0	6 555.1	6 721.8	6 441.1	5 483.6
Black, 7 iters.	2 625.0	2 582.3	2 988.4	2 618.6	2 143.1
Black, opt. (24)	1 413.2	1 462.6	1 906.1	1 490.1	1 193.7
Black, 50 iters.	1 304.8	1 384.6	1 839.7	1 421.1	1 126.3
FIXK, $q = 80\%$	83.1	83.9	272.7	141.9	105.4
Weickert, 7 iters.	14.5	15.4	102.2	39.1	33.3
Weickert, opt. (18)	6.5	8.0	79.8	26.9	21.4
Weickert, 50 iters.	5.5	6.9	76.5	25.1	19.7
FIXK, $q = 90\%$	3.6	3.8	25.9	8.8	6.2
ADAPTKLKR, opt. (7)	2.9	5.4	83.4	11.3	4.2
DIFIDEAL	2.0	1.8	9.0	3.8	3.6
FILTIDEAL	0.7	0.7	1.3	0.7	0.8

Table 3. The values of the characteristic $\mathrm{Var}(G) \times 10^{-3}$ in five region boundaries of type 2 in the MR-head phantom calculated for the output images of the individual GDD filtering methods.

GDD-f method	**Region boundary (case 2)**				
	B_1 ventricles	B_2 white matter	B_3 grey matter	B_4 CSF	B_5 fat
number of pixels	124	926	1140	724	704
original	347.9	339.9	119.3	31 552.6	3 739.8
Black, 7 iters.	286.9	311.7	94.6	31 573.6	3 328.2
Black, opt. (24)	258.9	303.7	85.5	31 599.8	3 156.2
Black, 50 iters.	259.5	302.6	85.0	31 600.7	3 060.8
FIXK, $q = 80\%$	196.7	274.2	61.5	31 560.8	2 822.6
Weickert, 7 iters.	171.3	267.3	51.9	31 768.2	2 728.9
Weickert, opt. (18)	162.4	264.6	49.7	31 785.2	2 642.7
Weickert, 50 iters.	158.4	264.1	49.1	31 776.0	2 591.5
FIXK, $q = 90\%$	107.1	265.3	46.2	31 115.8	2 498.0
ADAPTKLKR, opt. (7)	91.1	277.9	46.4	30 422.6	2 461.9
DIFIDEAL	79.4	236.0	29.5	31 308.6	2 440.7
FILTIDEAL	20.2	212.8	6.6	31 057.5	2 270.7

Table 4. The values of the characteristic $\mathrm{Var}(G) \times 10^{-3}$ in five region boundaries of type 3 in the MR-head phantom calculated for the output images of the individual GDD filtering methods.

GDD-f method	**Region boundary (case 3)**				
	B_1 ventricles	B_2 white matter	B_3 grey matter	B_4 CSF	B_5 fat
number of pixels	111	555	754	463	444
original	770.6	1 521.2	206.0	108 798.9	12 475.2
Black, 7 iters.	617.5	1 473.1	166.5	108 091.0	11 626.4
Black, opt. (24)	560.3	1 452.9	150.6	107 798.2	11 252.2
Black, 50 iters.	547.0	1 452.9	148.2	107 597.5	10 999.5
FIXK, $q = 80\%$	420.9	1 401.1	116.2	107 114.8	10 594.1
Weickert, 7 iters.	371.3	1 386.6	95.5	107 129.3	10 401.3
Weickert, opt. (18)	351.7	1 369.6	88.4	107 003.3	10 089.2
Weickert, 50 iters.	338.3	1 368.8	85.2	106 915.2	9 977.8
FIXK, $q = 90\%$	221.0	1 374.4	77.6	105 127.6	9 933.6
ADAPTKLKR, opt. (7)	215.4	1 656.0	80.5	101 316.4	9 803.9
DIFIDEAL	170.2	1 259.9	51.6	106 477.4	9 732.4
FILTIDEAL	80.7	1 196.2	25.1	106 207.2	9 416.1

images. In particular, a random variable G has been derived from the intensity gradient defined on selected image structures. The parameters of its chi-square distribution are estimated via maximum likelihood method adapted for the specific case of a stepwise constant image model corrupted by uncorrelated Gaussian noise. Inference of the explicit expression of probability distributions on *a-priori* known region boundaries of two types constitutes the essential part of the evaluation technique since it allows to derive the accurate ML estimates of the proposed image smoothing measure $\mathrm{Var}(G)$. The limitations given by the specific image model chosen and noise used are compensated by independence of this measure of numerical schemes for PDE solving and specific conductance selected.

The results presented in the Results subsection and discussion related to the MR-head phantom show that the values of $\mathrm{Var}(G)$ characterize the level of region interior homogenization satisfactorily. Further, the values of $\mathrm{Var}(G)$ proved to be a sensitive measure for characterization of staircase artifacts in the diffused images which have been evaluated in the literature only qualitatively up to now. A notion of gold standards for the GDD algorithms has been introduced for the phantom. These extremal cases of the GDD filtering serve as a sound basis for mutual quantitative comparison of the individual algorithms in the sense of the best reachable conductance values.

The quantitative evaluation results we obtained in a specific case of the MR-head phantom may be generalized for the algorithms based on other GDD filtering approaches in which a piecewise constant image phantom corrupted by uncorrelated Gaussian noise serves as a reasonable model of the actual image.

Table 5. The approximate ML estimators of the parameters of the chi-square distributions related to three studied cases.

Case	1	2	3
Distribution	$\frac{1}{2}\hat{\sigma}^2\chi_2^2$	$\frac{1}{2}\hat{\sigma}^2\chi_2'^2(\hat{\lambda})$	$\frac{1}{2}\hat{\sigma}^2\chi_2'^2(2\hat{\lambda})$
$\hat{\lambda}$	0	*eq.* (27)	*r.h.s.*(27)/2
$\hat{\sigma}^2$	$\overline{G}$	$2\overline{G}/(2+\hat{\lambda})$	$\overline{G}/(1+\hat{\lambda})$
$\widehat{E(G)}$	$\overline{G}$	$\frac{1}{2}\hat{\sigma}^2(2+\hat{\lambda})$	$\hat{\sigma}^2(1+\hat{\lambda})$
$\widehat{\mathrm{Var}(G)}$	$\overline{G}^2$	$\hat{\sigma}^4(1+\hat{\lambda})$	$\hat{\sigma}^4(1+2\hat{\lambda})$

Acknowledgements

The research was partially supported by the the Slovak Grant Agency for Science VEGA No. 1/0264/03

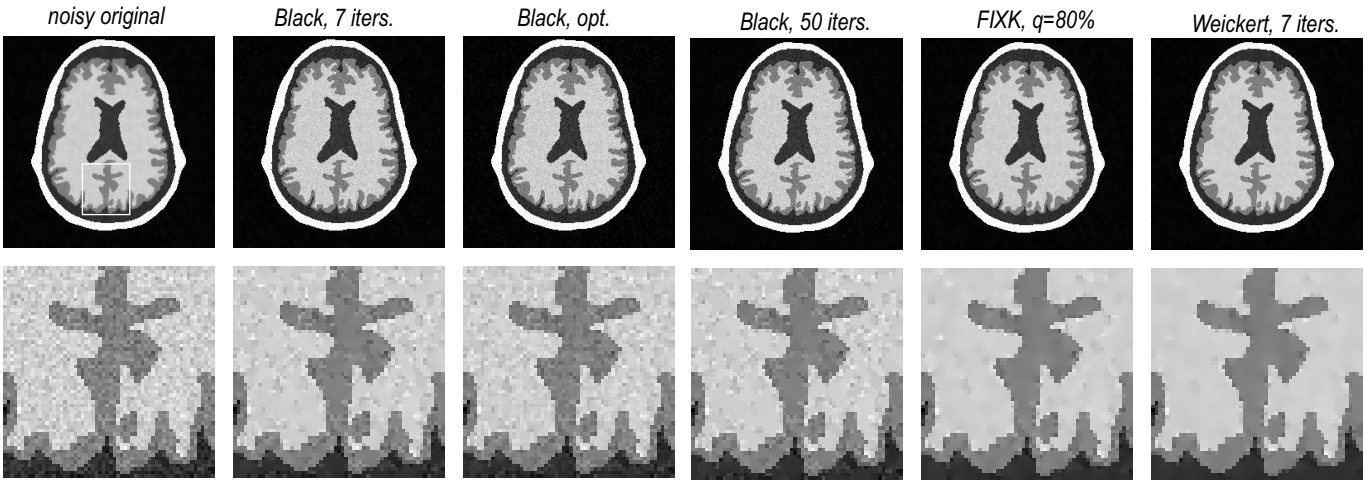

Fig. 4. Diffused phantom images and their fragments ordered according to the decreasing occurrence of staircase artifacts (part I).

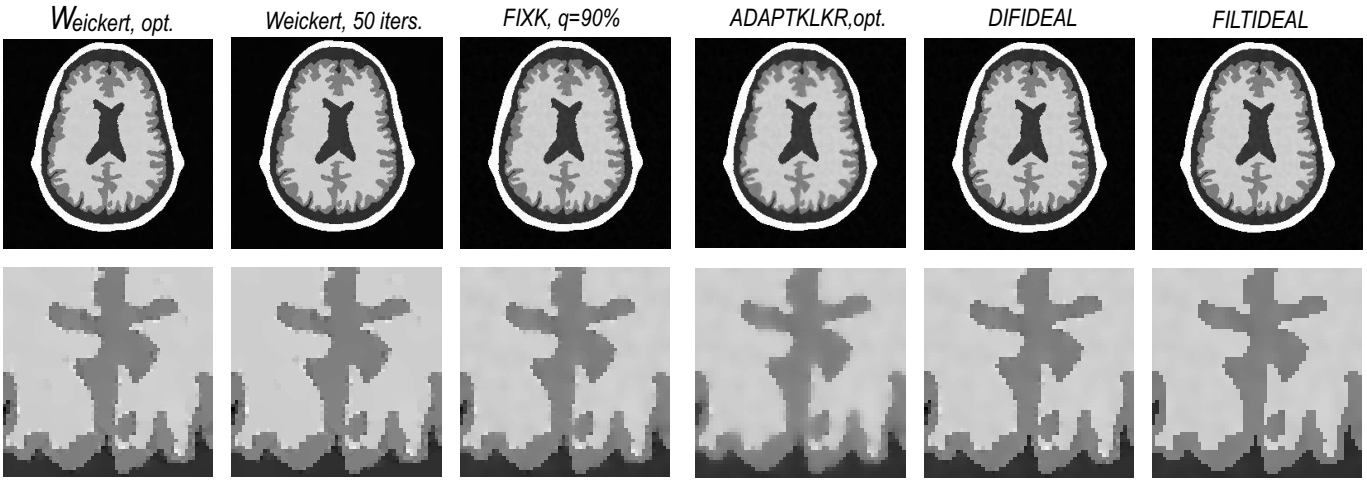

Fig. 5. Diffused phantom images and their fragments ordered according to the decreasing occurrence of staircase artifacts (part II).

APPENDIX

Maximum Likelihood estimates

In general, if $G_1, \ldots, G_n$ is a random sample from $\sigma^2\chi'^2_2(\lambda)$, and $\lambda = (\mu_1 - \mu_2)^2/\sigma^2$, then the maximum likelihood equations for λ and σ^2 are

$$\sum_{i=1}^{n} h\Big(\sqrt{(G_i/\hat\sigma^2)\hat\lambda}\Big)(G_i/\hat\sigma^2) = n\,, \quad \text{if } \overline{G} > \nu\sigma^2, \tag{13}$$

$$\hat\sigma^2 = \frac{\overline{G}}{(\nu + \hat\lambda)}\,, \tag{14}$$

where

$$\overline{G} = \frac{1}{n}\sum_{i=1}^{n} G_i\,, \tag{15}$$

$$h(z) = \frac{I_{\nu/2}(z)}{zI_{(\nu-2)/2}(z)}\,, \tag{16}$$

with $\nu = 2$. Here, the function $I_\nu(z)$ is the modified Bessel function of the first kind of order ν,

$$I_\nu(y) = (y/2)^\nu \sum_{j=1}^{\infty} \frac{(y^2/4)^j}{j!\Gamma(\nu + j + 1)}\,. \tag{17}$$

The ML equations (13) and (14) are modified (corrected) versions of (29.34a) and (29.34b) from Johnson ([30] p. 452), in accordance with Anderson [31].

In practical applications, to find the ML estimates $\hat\lambda$ and $\hat\sigma^2$, the original nonlinear system of ML equations (13) and (14) is to be solved, which have, in general setup $G_i \sim \sigma^2\chi'^2_2(\lambda)$ with separated variables, the form

$$\sum_{i=1}^{n} h\left(\sqrt{\left(\frac{G_i}{\overline{G}}\right)(2+\hat\lambda)\hat\lambda}\right)\left(\frac{G_i}{\overline{G}}\right)(2+\hat\lambda) - n = 0\,, \tag{18}$$

$$\hat\sigma^2 = \frac{\overline{G}}{(2+\hat\lambda)}\,. \tag{19}$$

For the numerical evaluation of the left-hand-side of the first equation, at any prior choice of $\lambda > 0$, it is reasonable to use a piecewise polynomial approximation of the function $h(z)$ for small z. For large z we propose to approximate $h(z)$ by the function

$$h_4(z) = z^{-1} - \frac{1}{2}z^{-2} - \frac{1}{8}z^{-3} - \frac{1}{8}z^{-4}. \qquad (20)$$

The application of the above results yields the following formulae for maximum likelihood equations of the parameters:

Case 1 ≡ 4: For this case, $G_1, \ldots, G_n$ represent a random sample from central chi-square distribution, *ie* $\lambda = 0$, $G_i \sim (\frac{1}{2}\sigma^2)\chi_2^2$, for $i = 1, \ldots, n$. Then $\hat{\lambda} = 0$ and $\hat{\sigma}^2 = \overline{G}$. The ML estimator of the expected value of G is $\widehat{E(G)} = \hat{\sigma}^2$ and the estimator of the variance is $\widehat{\mathrm{Var}(G)} = \hat{\sigma}^4$.

Case 2: Here, $G_1, \ldots, G_n$ represent a random sample from noncentral chi-square distribution, $G_i \sim (\frac{1}{2}\sigma^2)\chi_2'^2(\lambda)$, with $\lambda = (\mu_1 - \mu_2)^2/(2\sigma^2)$, for $i = 1, \ldots, n$. The ML estimates are given as a solution of the system (18), (19), in which r.h.s./2 is to be used.

Further, we can introduce

$$\widehat{(\mu_1 - \mu_2)}^2 = 2\hat{\lambda}\hat{\sigma}^2, \qquad (21)$$

as the ML estimator of the squared difference between mean values of Ω_1 and Ω_2. The estimators of mean and variance are $\widehat{E(G)} = \frac{1}{2}\hat{\sigma}^2(2+\hat{\lambda})$ and $\widehat{\mathrm{Var}(G)} = \hat{\sigma}^4(1+\hat{\lambda})$.

Case 3: Finally, let $G_1, \ldots, G_n$ represent a random sample from noncentral chi-square distribution, $G_i \sim (\frac{1}{2}\sigma^2)\chi_2'^2(2\lambda)$, with $\lambda = (\mu_1 - \mu_2)^2/(2\sigma^2)$, for $i = 1, \ldots, n$. The ML estimates are given as a solution of the system

$$\sum_{i=1}^{n} h\Big(\sqrt{\Big(\frac{G_i}{\overline{G}}\Big)(2+2\hat{\lambda})2\hat{\lambda}}\Big)\Big(\frac{G_i}{\overline{G}}\Big)(2+2\hat{\lambda}) - n = 0, \qquad (22)$$

$$\hat{\sigma}^2 = \frac{2\overline{G}}{(2+2\hat{\lambda})}. \qquad (23)$$

Moreover, we have

$$\widehat{(\mu_1 - \mu_2)}^2 = 2\hat{\lambda}\hat{\sigma}^2, \qquad (24)$$

and the remaining estimators $\widehat{E(G)} = \hat{\sigma}^2(1+\hat{\lambda})$, and $\widehat{\mathrm{Var}(G)} = \hat{\sigma}^4(1+2\hat{\lambda})$.

Anderson [31] showed that if σ^2 is unknown but greater than a small positive number, then there is a unique explicit solution to the likelihood equations (asymptotic properties of the estimators are given in [30] and in [32].

For large z, the function $h(z)$ given by (16) can be sufficiently well approximated by $h_2(z) = z^{-1} - \frac{1}{2}z^{-2}$. Then the function $h(z)$ may be utilized for derivation of explicit expression of parameter estimates. They can considerably simplify the computations in applications with sufficiently large values of the argument z. If $G_i \sim \sigma^2\chi_2'^2(\lambda)$, $i = 1, \ldots, n$, then using $h_2(z)$ instead of $h(z)$ and from (18), we get the quadratic equation for $\hat{\lambda}$:

$$4(a-1)\hat{\lambda}^2 + 4(2a-1)\hat{\lambda} - 1 = 0 \qquad (25)$$

where $a = \tilde{G}/\overline{G}$, $\overline{G}$ is given by (15), and

$$\tilde{G} = \left(\frac{1}{n}\sum_{i=1}^{n}\sqrt{G_i}\right)^2. \qquad (26)$$

The maximum positive root of the equation (25) is the approximate ML estimate of λ.

In particular, solving equation (25) and using (19) we get the explicit (approximate) formulae for ML estimators of λ and σ^2 in general case:

$$\hat{\lambda} = \frac{-(1-2a) + \sqrt{a(4a-3)}}{2(1-a)} \qquad (27)$$

$$\hat{\sigma}^2 = \frac{\overline{G}}{(2+\hat{\lambda})}. \qquad (28)$$

Application of the above results leads to the approximate formulae for maximum likelihood estimates of the parameters (cases 1–3) which are summarized in Table 5.

References

[1] Ter Haar Romeny,B.M. (ed): Geometry-Driven Diffusion in Computer Vision, Kluwer Academic Publishers, Dordrecht, 1994.

[2] CASELLES, V,—MOREL, J-M.—SAPIRO, G.—TANNENBAUM, A.(eds): Special Issue on Partial Differential Equations and Geometry-Driven Diffusion in Image Processing and Analysis, IEEE Trans on Image Processing **7** (1998), 269–475.

[3] WEICKERT, J.—ter HAAR ROMENY, B. M.—VIERGEVER, M. A.: Efficient and Reliable Schemes for Nonlinear Diffusion Filtering, IEEE Trans. on Image Processing **7** (1998), 398–410.

[4] CATTÉ, F.—LIONS, P-L.—MOREL, J-M.—COLL, T.: Image Selective Smoothing and Edge Detection by Nonlinear Diffusion, SIAM J. Num. Anal. **29** (1992), 182–193.

[5] ALVAREZ, L.—LIONS, P.-L.—MOREL, J.-M.: Image Selective Smoothing and Edge Detection by Nonlinear Diffusion II., SIAM J. Num. Anal. **29** (1992), 845–866.

[6] WEICKERT, J.: Theoretical Foundations of Anisotropic Diffusion in Image Processing, Computing Suppl. **11** (1996), 221–236.

[7] GERIG, G.—KÜBLER, O.—KIKINIS, R.—JOLESZ, F. A.: Nonlinear Anisotropic Filtering of MRI Data, IEEE Trans. on Medical Imaging **11** (1992), 221–232.

[8] LI, X.—CHEN, T.: Nonlinear Diffusion with Multiple Edginess Thresholds, Pattern Recognition **27** (1994), 1029–1037.

[9] NIESSEN, W. J.—ter HAAR ROMENY, B. M.: Numerical Analysis of Geometry-Driven Diffusion Equations, In: Geometry-Driven Diffusion in Computer Vision, Kluwer Academic Publishers, Dordrecht, 1994, pp. 393–410.

[10] BAJLA, I.—HOLLÄNDER, I.: Nonlinear Filtering of Magnetic Resonance Tomograms by Geometry-Driven Diffusion, Machine Vision and Applications **10** (1998), 243–255.

[11] LIU, X.—KANUNGO, T.—HARALICK, R. M.: In: Proc. of the DARPA Image Understanding Workshop, Palm Springs, CA, February 1996. II, pp. 1533–1540.

[12] Report on IEEE Computer Society Workshop on Empirical Evaluation of Computer Vision Algorithms, Santa Barbara, CA, June 1998, http:/www.itl.nist.gov/iaui/vip/2eecv/cvpr98-report.html.

[13] PHILLIPS, P. J.—BOWYER, K. W. (eds): Special Issue on Empirical Evaluation of Computer Vision Algorithms, IEEE Trans. on Pattern Analysis and Machine Intelligence **21** No. 4 (1999), 289–384.

[14] PERONA, P.—MALIK, J.: Scale-Space and Edge Detection Using Anisotropic Diffusion, IEEE Trans. on Pattern Analysis and Machine Intelligence **12** (1990), 629–639.

[15] OTTENBERG, K.: Model-Based Extraction of Geometric Structure from Digital Images, 1993, PhD Dissertation. The University of Utrecht, Utrecht.

[16] DER-SHAN LUO—KING, M. A.—GLICK, S.: Local Geometry Variable Conductance Diffusion for Post-Reconstruction Filtering, IEEE Trans. Nucl. Sci. **41** No. 6 (1994), 2800–2806.

[17] WEICKERT, J.: Anisotropic Diffusion Filters for Image Processing Based Quality Control, In: Fasano, A., Primicerio, M. (eds), Proc. of the Seventh European Conf. on Mathematics in Industry, B.G. Teubner, Stuttgart, 1994, pp. 355–362.

[18] YU-LI YOU—XU, W.—TANNENBAUM, A.—KAVEH, M.: Behavioral Analysis of Anisotropic Diffusion in Image Processing, IEEE Trans. on Medical Imaging **5** (1996), 1539–1553.

[19] BLACK, M. J.—SAPIRO, G.—MARIMONT, D. H.—HEEGER, D.: Robust Anisotropic Diffusion, IEEE Trans. on Image Processing **7** (1998), 421–432.

[20] WEICKERT, J.: Anisotropic Diffusion in Image Processing, B.G. Teubner, Stuttgart, 1998.

[21] MONTEIL, J.—BEGHDADI, A.: A New Interpretation and Improvement for the Nonlinear Anisotropic Diffusion for Image Enhancement, IEEE Trans. on Pattern Analysis and Machine Intelligence **21** No. 9 (1999), 940–946.

[22] BAJLA, I.—HOLLÄNDER, I.: Locally Adaptive Conductance in Geometry-Driven Diffusion Filtering of Magnetic Resonance Tomograms, IEE Proceedings–Vision, Image and Signal Processing **147** (2000), 271–282.

[23] SARTI, A.—MIKULA, K.—SGALLARI, F.: Nonlinear Multiscale Analysis of Three-Dimensional Echocardiographic Sequences, IEEE Trans. on Medical Imaging **18** No. 6 (1999), 453–466.

[24] DIEWALD, U. PREUSSER, T.—RUMPF, M.: Anisotropic Diffusion in Vector Field Visualization on Euclidean Domains and Surfaces, IEEE Trans. on Visualization and Computer Graphics **6** (2000), 139–149.

[25] YUE WANG—TIANHU LEI: A New Stochastic Model-Based Image Segmentation Technique for MR Image of MR Imaging and its Application in Image Modeling, In: Proc. of the IEEE Int. Conf. on Image Processing and Neural Networks, Austin, TE, November 1994, I, pp. 182–186.

[26] SIJBERS, J,—den DEKKER, A. J.—VAN AUDEKERKE, J.—VERHOYE, M.—VAN DYCK, D.: Estimation of the Noise in Magnitude MR Images, Magnetic Resonance Imaging **16** (1998), 87–90.

[27] NOWAK, R. D.: Wavelet-Based Rician Noise Removal for Magnetic Resonance Imaging, IEEE Trans. on Image Processing **8** (1999), 1408–1418.

[28] BAJLA, I.—HOLLÄNDER, I.: Geometry-Driven Diffusion Filtering of Magnetic Resonance Images Using Model-Based Conductance, Machine Vision and Applications **12** (2001), 223–237.

[29] LINDEBERG, T.—ter HAAR ROMENY, B. M.: Linear Scale-Space II: Early Visual Operations, In: Geometry-Driven Diffusion in Computer Vision, Kluwer Academic Publishers, Dordrecht, 1994, pp. 39–72.

[30] JOHNSON, N. L.—KOTZ, S.—BALAKRISHNAN, N.: Continuous Univariate Distributions. Volume 2, Second Edition, Wiley, New York, 1995.

[31] ANDERSON, D. A.: The Circular Structural Model, J. Royal Stat. Soc., Series B **43** (1981), 131–143.

[32] ANDERSON, D. A.: Maximum Likelihood Estimation in the Noncentral Chi-Distribution with Unknown Scale Parameter, Sankhya: The Indian J. Stat., Series B **43** (1981), 58–67.

Received 5 November 2002

Ivan Bajla (RNDr, Ing (MSc), PhD), received his PhD degree in measurement science (biomeasurement and image processing) from the Institute of Measurement Theory of the Slovak Academy of Sciences (SAS) in Bratislava, Slovak Republic in 1977, and RNDr degree from Comenius University in Bratislava in 1980. From 1977 till 1980 he was on leave at the Joint Institute for Nuclear Research in Dubna, USSR. His research interests include image reconstruction from projections, orthogonal and gray-scale transformations of digital images, non-linear diffusion methods of image filtering and segmentation, especially in the field of MR and CT imaging and visualization. In the periods of time: 1985-91, 1993-98 he was in charge of Image Processing Department of the Institute of Measurement Science, Slovak Academy of Sciences. At present he is with the High Performance Image Processing Department of the Austrian Research Centers in Seibersdorf.

Igor Holländer (Ing (MSc), PhD), joined the Institute of Measurement Science of the Slovak Academy of Sciences in Bratislava, Slovakia, in 1985. From 1986 to 1988 he studied computer science at Comenius University in Bratislava. In 1990 he received his PhD degree in measurement science (biomeasurement and image processing) from the Institute of Measurement Science, Slovak Academy of Sciences. From 1991 to 1992 he was Head of the Image Processing Department of the SAS. From 1992 to 1998 he worked as a research fellow at the Institute of Information Processing of the Austrian Academy of Sciences in Vienna, Austria. In 1998, he became a lecturer in functional magnetic resonance imaging at the University of Manchester, UK. From 2001, he works with the High Performance Image Processing Department of the Austrian Research Centers. His research interests include medical visualization and graphics, medical imaging and image processing, in particular functional neuroimaging.

Viktor Witkovský (RNDr, PhD), received his PhD degree in mathematical and physical sciences (probability and mathematical statistics) from the Faculty of Mathematics and Physics, Comenius University, Bratislava, Slovakia, in 1993. He joined the Institute of Measurement Science of the Slovak Academy of Sciences in Bratislava in 1986. From 1995 he is Head of the Department of Theoretical Methods at the Institute. In 1997 he was awarded the Ruth Crawford Mitchell Scholarship from Nationality Rooms at the University of Pittsburgh, USA. Currently his research interests include inference in stochastic models with complicated variance-covariance structure.